NANOSTRUCTURED MATERIALS AND FUNCTIONAL COATINGS

Effect of Nitrogen Concentration in a Gas Mixture on the Structure and Properties of Zr–B–(N) Coatings Obtained by the HIPIMS Methods

A. D. Sytchenko[a], *, S. B. Kabildina[a], **, and Ph. V. Kiryukhantsev-Korneev[a], ***

[a] National University of Science and Technology MISIS, Moscow, 119049 Russia
*e-mail: alina-sytchenko@yandex.ru
**e-mail: kabildinas@mail.ru
***e-mail: kiruhancev-korneev@yandex.ru

Abstract—Zr–B–N coatings have been obtained by high-power impulse magnetron sputtering (HIPIMS) in Ar, Ar + 15% N_2, and N_2 gaseous media using a ZrB_2 target made by self-propagating high-temperature synthesis (SHS). Sputtering is carried out at the following parameters: mean power of 1 kW, peak power of 70 kW, peak current of 130 A, frequency of 100 Hz, and pulse duration of 200 μs. The working pressure in the vacuum chamber is 0.1–0.2 Pa, the distance between the substrate and the target is 80 mm, and the coating deposition time is 40 min. Glass, silicon, and high-speed steel are used as substrates. For comparison with the HIPIMS method, the coatings are also applied by direct current magnetron sputtering (DCMS) at an average power of 1 kW. The composition and structure of the coatings are studied by scanning electron microscopy (SEM), glow discharge optical emission spectroscopy (GDOES), Raman spectroscopy, Fourier-transform infrared spectroscopy (FTIR), and X-ray diffraction (XRD) analysis. The mechanical, tribological, and optical properties of Zr–B–N coatings, as well as the resistance to dynamic impact loading, are studied. All coatings are characterized by a dense structure and the absence of columnar grains. With the help of spectroscopic structural studies of the coatings, it is revealed that, during deposition in a reaction medium, the BN phase is formed, which has a significant effect on the microstructure and characteristics of the coatings. An increase in the nitrogen concentration in the gas mixture during the deposition of Zr–B–N coatings leads to an increase in the optical transmittance of the coatings up to 97%, resistance to cyclic dynamic impact loads by 40%, and a decrease in the starting value of friction coefficient by 60%. The nonreactive coating is found to have a maximal hardness of 19 GPa and elastic modulus of 221 GPa.

Keywords: HIPIMS, coatings, Zr–B–N, optical properties, mechanical and tribological characteristics

INTRODUCTION

Ceramic materials based on zirconium diboride are used in the production of metal-working equipment, components of microelectronic devices, the aerospace industry, and other fields due to their high melting point of 3027°C [1, 2], low resistivity of 4.6 μΩ cm [3], high thermal stability [4] and resistance to oxidation to 1200°C [5], hardness of about 35–45 GPa, Young's modulus from 350 to 400 GPa, and elastic restitution of 70% [6]. Coatings based on ZrB_2 show a high absorption factor of 0.92 and low emission factor of 0.11 [7], and can be used as spectrally selective optical coatings [8, 9].

Mechanical, tribological, and optical properties of ZrB_2 coatings can be modified by the controlled introduction of nitrogen atoms into the composition during deposition in the reaction medium or straight into the target material [10, 11]. The addition of nitrogen is known to enhance the optical features of ZrB_2 coatings: transmittance may achieve 99–100% due to the formation of the BN phase [12]. The amorphization of the coatings caused by the insertion of nitrogen in ZrB_2 leads to the appearance of interference colors, which enables decorative usage [13].

The barrier layer of Zr–B–N efficiently blocks the mutual diffusion of copper and silicon atoms at temperatures below 650°C, which may be of use in microelectronic devices [14]. Zr–B–N coatings are also used in metal cutting, since they show high wear resistance and do not form chips and thermal cracks during operation [15]. As the nitrogen content grows, the hardness of Zr–B–N coatings slightly decreases, but their resistance to corrosion increases [13, 16].

The development of these coatings requires an investigation into their tribological properties in the sliding friction regime and under dynamic impact

loading, which simulates the interaction of the surface of an instrument and a treated element or impact influence of abrasive particles on optical devices (solar cells, windows, etc.).

Direct-current magnetron sputtering (DCMS) is the most widely used method for obtaining Zr−B−N coatings [10, 14]. The advantages of this method are as follows:

—low density of defects on the coating [17];

—versatile character (coatings may be deposited onto almost any material) [18, 19].

One of the main drawbacks of DCMS is the relatively low adhesive strength of the resulting films, which is due to the low ionization degree of the flow, typically below 1% [20].

The use of the high-power impulse magnetron sputtering (HIPIMS) method allows improving the adhesive strength of the coatings by increasing the plasma density, which ionizes the atoms knocked out from the target and leads to an increase in the flow ionization degree [20]. In addition, an increased density of the coatings created by the HIPIMS technology enhances their mechanical and tribological characteristics and thermal and corrosion resistance [21−23].

The aim of this work was to obtain Zr−B−N coatings by HIPIMS with a varied N_2 content in the gas medium and an investigation into their structure and optical, mechanical and tribological characteristics, as well as of the resistance to dynamic impact load. Positive effects were found which appear in the HIPIMS technology as compared to DCMS.

EXPERIMENTAL

The deposition of coatings by the HIPIMS method was performed on a modernized magnetron sputtering apparatus based on the vacuum system UVN-2M (Russia). Magnetrons and an ion source with slit aperture are mounted in the vacuum chamber. The target made of ZrB_2 was used for sputtering; the target was prepared by self-propagating high-temperature synthesis (SHS). The process was carried out in Ar (99.9995%), N_2 (99.999%), and the mixture Ar + 15% N_2 with the following parameters:

— average power 1 kW,

— peak power 70 kW,

— peak current 130 A,

— frequency 100 Hz,

— pulse duration 200 μs,

— working pressure in the vacuum chamber 0.1−0.2 Pa,

— distance between the substrate and the target 80 mm,

— deposition process duration 40 min.

To compare the efficiencies of two technologies, the films were also obtained by the DCMS method with the following parameters:

— current 2 A,

— voltage 500 V,

— power 1 kW,

— deposition process duration 40 min.

The substrate was made from silicon of the KEF-4.5 type (100) in structural and mechanical studies, glass for determining the optical properties, and R18 high-speed steel for tribological tests. The substrates were cleaned by sonication in isopropanol on an UZDN-2T sonicator at the frequency of 22 kHz for 3 min. Before deposition by the HIPIMS and DCMS methods, the substrates were subject to ion etching with argon ions for 10 min using the ion source working at the acceleration voltage of 2 kV and current of 70 mA.

Structural studies of the films were conducted by scanning electron microscopy (SEM) using an S-3400N instrument equipped with a NORAN 7 unit for energy dispersive spectroscopy (EDS) (Hitachi, Japan). Optical microanalysis (OM) of the coating surface was carried out on an AXIOVERT 25CA microscope (Carl Zeiss, Germany). Elemental analysis was performed by glow discharge optical emission spectroscopy (GDOES) on a Profiler 2 instrument (Horiba Jobin Yvon, France). X-ray diffraction (XRD) studies of the films were carried out using CuK_α radiation on a Phaser D2 diffractometer (Bruker, Germany). Raman scattering spectra were obtained on an NTEGRA instrument (NT-MDT, Russia) equipped with a red laser (wavelength 633 nm).

Infrared spectroscopy was performed in the reflection mode at the angle of 120° in the wavenumber range from 400 to 4000 cm^{-1} on a Vertex 70 vacuum FTIR spectrometer (Bruker). Transmittance was determined on a KFK-3 spectrometer (Russia) by comparing the studied coating with the uncoated substrate in the wavelength range of 350−950 nm.

Hardness (H), Young's modulus (E), elastic restitution (W), plasticity index (H/E), and the resistance to plastic deformation index (H^3/E^2) of the coatings were estimated by a Nano-Hardness Tester (CSM Instruments, Switzerland); the indenter was loaded by the force of 4 mN. Tribological tests were made on an automated Tribometer instrument (CSM Instruments) at a speed of 10 cm/s and under the following conditions:

— counterbody SUS316 (stainless steel), load 2 N;

— counterbody 100Cr6 (roller-bearing steel), load 5 N.

Resistance to cyclic dynamic impact loads was tested by an Impact Tester device (CemeCon, Germany) at loads of 100 and 300 N and the constant frequency of 50 Hz. The number of impacts was 10^5. The size of the wear tracks and craters after tribological and

Table 1. Elemental composition of coatings

Sample no.	Medium	Composition, at %			Thickness, μm	Growth rate, μm/min
		Zr	B	N		
1	Ar	28.9	71.1	–	1.6	0.04
2	Ar + 15% N₂	12.5	38.0	49.5	1.5	0.0375
3	N₂	18.2	13.0	68.8	0.1	0.0025

dynamic tests was estimated by optical profilometry on a WYKO-NT1100 device (Veeco, United States).

RESULTS AND DISCUSSION

Table 1 presents the elemental composition averaged over the thickness of the coatings. The content of the main elements in sample *1* was 28.9 at % Zr and 71.1 at % B. As the partial pressure of nitrogen increased, the concentration of Zr and B decreased by 56 and 46%, respectively, in sample *2* and by 37 and

82% in sample *3*. The fraction of nitrogen was 49.5 and 68.8 at % for films *2* and *3*, respectively.

Profiles of the elements distribution over the thickness of the coatings *1–3* deposited onto the R18 substrates are shown in Fig. 1.

Evidently, all elements are uniformly distributed inside the coatings. The thickness values and growth rates of the coatings, determined by GDOES, are listed in Table 1. The decrease in these parameters with increased nitrogen content in the gas phase may be due to the low ionization degree of nitrogen com-
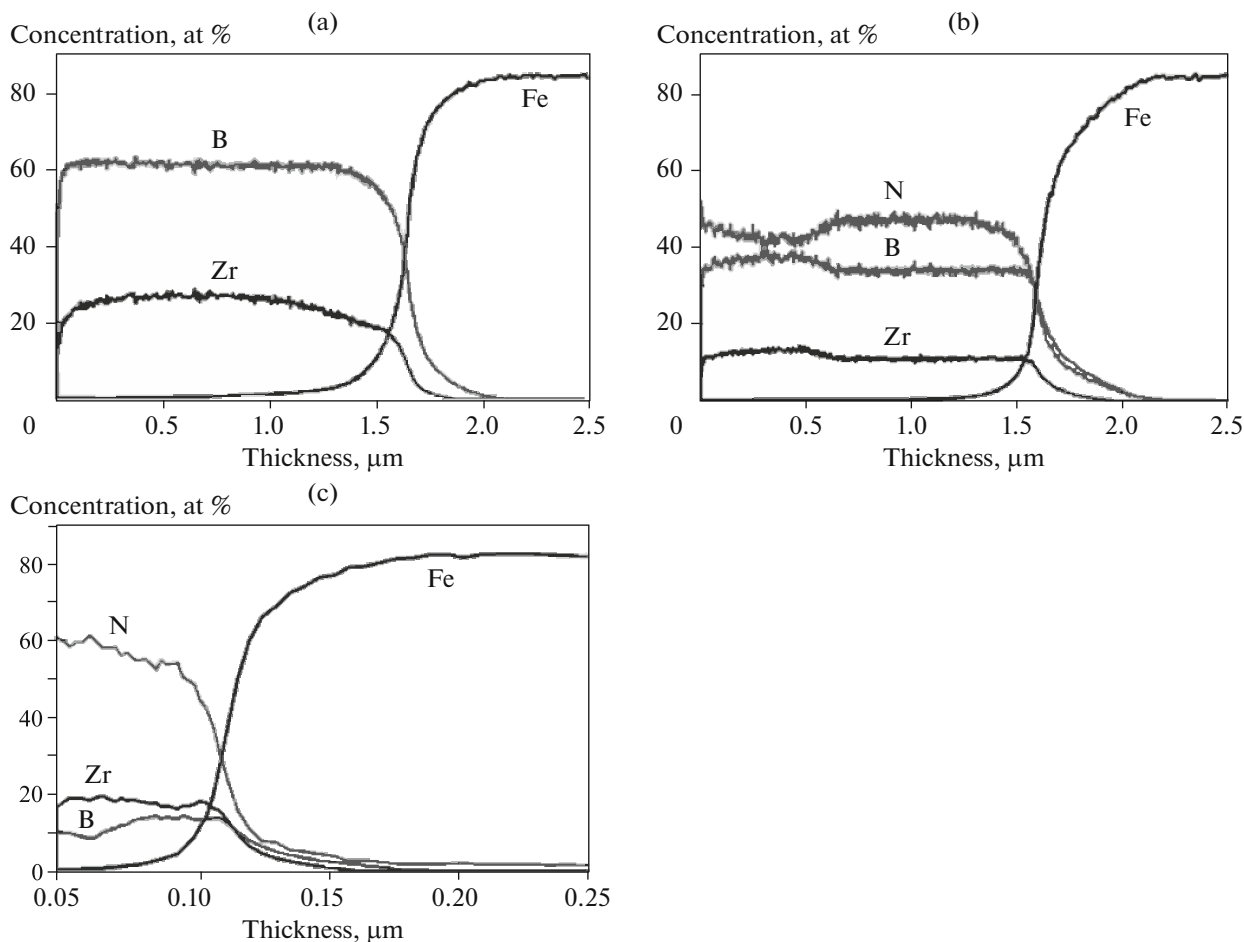
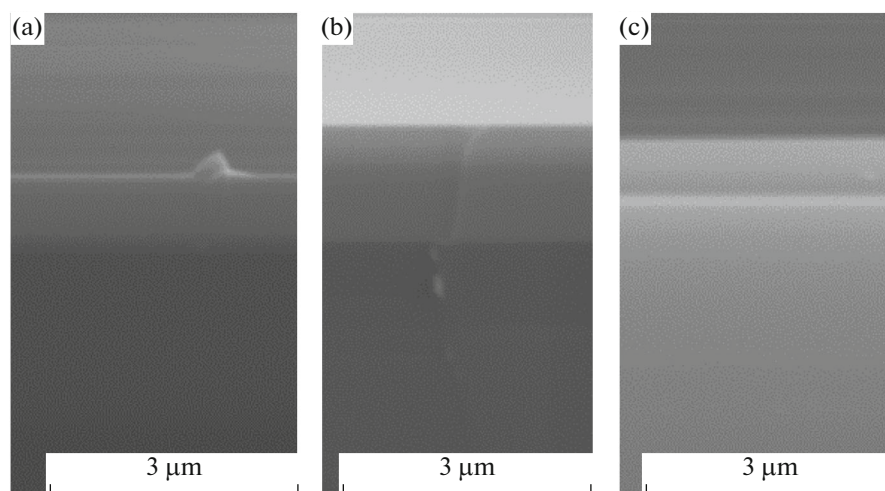**Fig. 1.** GDOES profiles of coatings (a) *1*, (b) *2*, and (c) *3*.

Fig. 2. Cross-section SEM images of coatings (a) *1*, (b) *2*, and (c) *3* deposited in (a) Ar, (b) Ar + 15% N$_2$, and (c) N$_2$.

pared to argon and by the target poisoning by nitrogen atoms [10, 17].

According to the SEM data (Fig. 2), all HIPIMS films possessed dense structure without prominent columnar elements.

The thickness determined from the SEM images of the films *1–3* grown on Si substrates was found to be 0.8, 1.4, and 0.5 μm, respectively. The difference between the values obtained by SEM and GDOES can be explained by a higher roughness degree of the R18 substrate and by a strong strain, exfoliation, and repeated deposition of the coating in the case of the Si substrate. Note that usually ZrB$_2$ films obtained by DCMS have a columnar structure, which has a negative effect on their properties. No columnar growth was observed in our case.

An analysis based on optical microscopy showed that Zr–B–N coatings, which had been deposited
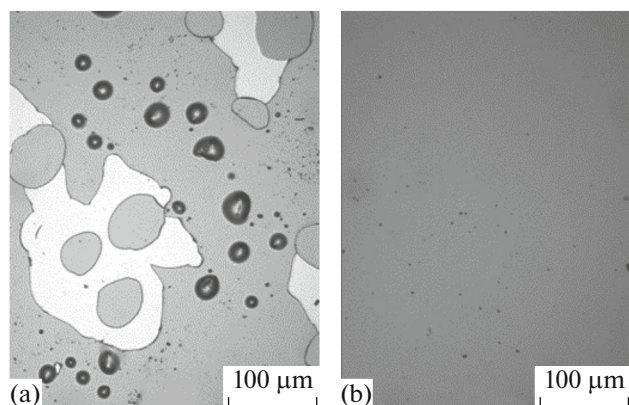

Fig. 3. Optical microscopy data on the microstructure of the coating obtained in the Ar + 15% N$_2$ environment by (a) DCMS and (b) HIPIMS.

onto silicon substrates by DCMS [25], had exfoliated areas. This indicates low adhesion strength of the coatings (Fig. 3a). Samples obtained by the HIPIMS method demonstrated a high degree of continuity and few surface defects (Fig. 3b).

Diffraction patterns of all coatings (Fig. 4) contained peaks from the substrate components (Fe and WC). The sample obtained in the Ar medium contained the hexagonal phase ZrB$_2$ (ICDD 034-0423). The grain size was 9 nm, as followed from the Debye–Scherrer equation applied to the most intensive line (001). Nitrogen-containing films did not give rise to peaks of ZrB$_2$; only a broad peak in the angle range $2\theta = 25°–35°$ remained, which can be attributed to the presence of an amorphous phase. Note that this phase can be characterized by the presence of B–N and Zr–N bonds, because lines of the maximal intensity of the BN phase (ICDD 085-1068) and ZrN (ICDD 035-0753) fall into the mentioned 2θ angle range. X-ray diffraction spectrum of the sample *3* did not show any peaks from the coating, probably due to its very small thickness of about 100 nm. Thus, the introduction of nitrogen into the composition of the films resulted in amorphization and a decrease in the grain size. A similar effect was observed in [24, 26, 27] as well.

Results of the Raman scattering studies are presented in Fig. 5. Peaks of ZrB$_2$ observed from coatings obtained in Ar and N$_2$ media are located at $\nu \sim 200$ and $500–600$ cm^{-1} [28]. Sample *2* showed peaks at $\nu = 169, 230$, and 510 cm^{-1}, which can be assigned either to the phase ZrB$_2$ or ZrN [29]. A broadened peak at $\nu = 1300–1500$ cm^{-1} proves the presence of the boron nitride phase, since it is characterized usually by signals at $\nu = 1200, 1365$, and 1381 cm^{-1} [30–32]. In the range of $\nu = 800–879$ cm^{-1}, peaks appear which prob-

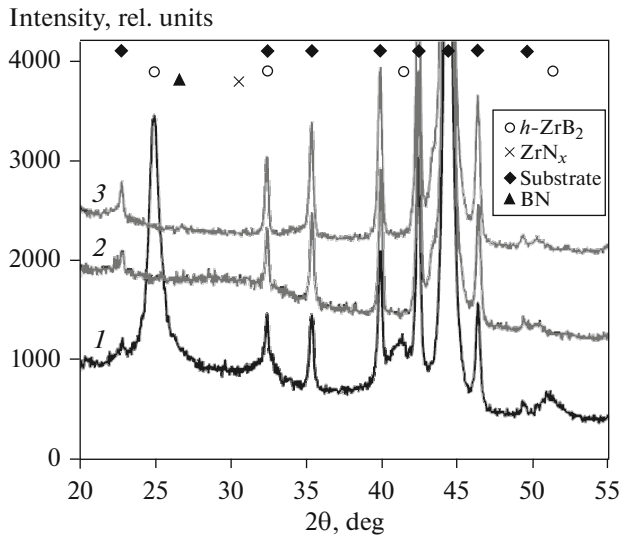**Fig. 4.** XRD patterns of coatings deposited in (*1*) Ar, (*2*) Ar + 15% N_2, and (*3*) N_2.

Fig. 5. Raman spectra of coatings.

ably belong to the phase of B_3OH_3 [33, 34] arising due to interaction of boron-containing phases of the coating with the atmospheric oxygen and water vapor on the sample surface. Only peaks from the Si substrate at $\nu = 300$, 520, 810, and 970 cm^{-1} [35−37] were revealed for sample *3*, which is explained by its small thickness of ~0.1 μm.

Infrared spectroscopic data on the studied films are shown in Fig. 6. Two signals at $\nu \sim 800$ and 1500 cm^{-1} were observed for sample *2*, which point to the formation of B−N bonds [38]. Since these bonds appear in the spectroscopic data but no peaks from crystalline BN are observed in the XRD data, we can conclude that the BN phase is amorphous.

Optical studies revealed that samples *1* and *2* obtained in Ar and Ar + 15% N_2 had an optical transmission coefficient of 20% at the wavelength $\lambda = 350$ nm, which decreased to zero as λ increased. Coating *3* showed a constant transparency level in the wavelength range from 350 to 950 nm; its average value was 97%. Increasing nitrogen content during the deposition process of Zr–B−N coatings was found to increase optical transmittance, which is explained by the decreased thickness of the films and the growing content of the BN phase possessing a nonmetallic bond character [12, 39].

Results of nanoindentation and tribological tests are listed in Table 2.

Values of H/E and H^3/E^2 were determined to predict the behavior of the coatings under the conditions of sliding friction and dynamic impact loading. Note that sample *1* demonstrated the highest hardness (19 GPa) and elastic modulus (221 GPa). The hardness decreased by 47% upon the addition of nitrogen;
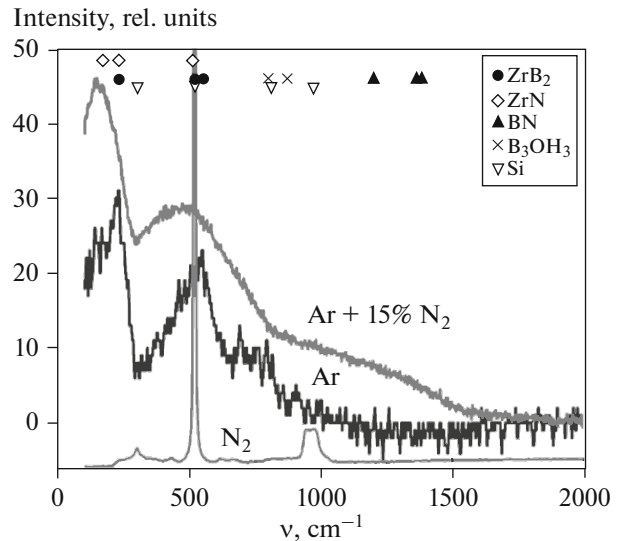
the corresponding loss in the elastic modulus was 37%; in the ratio H/E, 15%; and, in the ratio H^3/E^2, 64%. Elastic restitution increased 80% at the same time. An analogous decrease in the mechanical properties was also observed in [10, 13, 16], which was attributed to the formation of the soft amorphous BN phase in nitrogen-containing films.

A comparison of the features of coatings obtained in Ar in the DCMS and HIPIMS modes showed that in the first case the hardness of the samples was 22 GPa, and their elastic modulus was 342 GPa. These values are 16 and 55% higher than those for the sample *1* (HIPIMS) [25]. If the DCMS method is used in the atmosphere Ar + 15% N_2, we obtain $H = 23$ GPa and $E = 266$ GPa, which exceed the properties of the
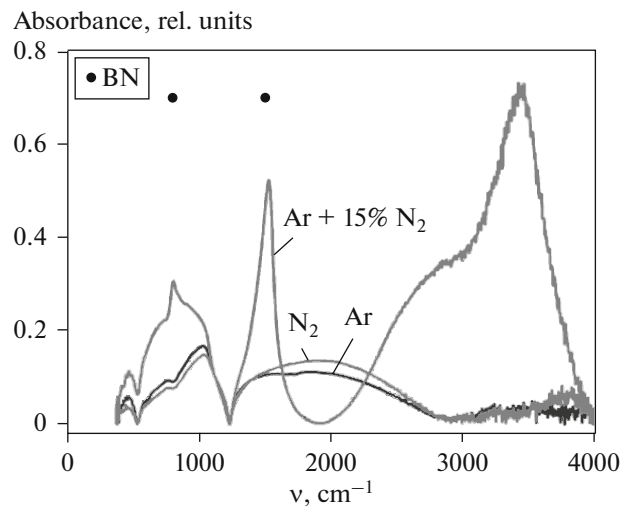

Fig. 6. Results of FTIR spectroscopy of coatings.

Table 2. Mechanical and tribological properties of coatings

Sample no.	Medium	Mechanical properties					Tribological properties	
							μ_0	
		H, GPa	E, GPa	W, %	H/E	H^3/E^2, GPa	SUS316	100Cr6
1	Ar	19	221	41	0.085	0.14	0.207	0.165
2	Ar + 15% N_2	13	147	64	0.088	0.10	0.212	0.145
3	N_2	10	139	74	0.072	0.05	0.085	0.165

HIPIMS films by 77 and 81%, respectively. This difference may be related to the decreased growth rate of the coatings in the HIPIMS mode, which leads to a reduction of internal stress and increasing content of oxygen and nitrogen impurities. This, in turn, has a negative effect on the mechanical properties.

Table 2 presents the initial friction coefficient μ_0 for the coatings using SUS316 and 100Cr6 steels as the counterobjects at loads of 2 and 5 N, respectively. In the case of SUS316 and a load of 2 N, the initial friction coefficient for the substrate is 0.258; for sample *1* it was found to be $\mu_0 = 0.207$. If the nitrogen medium was used, the value of μ_0 decreased by ~60%. In the case of 100Cr6 and the force of 5 N, the initial friction coefficients for the coatings *1* and *3* were 0.165, which is close to the value of 0.166 found for the substrate. Coating *2* deposited in the mix Ar + 15% N_2 showed the smallest $\mu_0 = 0.145$. Thus, the lowest friction coefficients in contact with the counterobjects SUS316 and 100Cr6 belong to the nitrogen-containing coat-

ings. This may be due to the BN phase, which serves as a solid lubricant [40].

Dynamic impact loading tests showed that no wearing signs appear on the coating surface at a weak load of 100 N. The destruction of the surface is detected only for the uncoated substrate (crater volume $V = 2.16 \times 10^3$ μm^3). Data on the investigation into wearing craters after testing with a load of 300 N are shown in Fig. 7.

Brittle failure in the crater was observed for the nonreactive coating, whereas nitrogen-containing coatings were characterized by wearing products accumulated on the boundaries of the tribocontact zone. Table 3 presents the results of calculation of the width (B), depth (D), and crater volume (V) after a dynamic impact test with a load of 300 N.

We can conclude that addition of nitrogen leads to an increased resistance to the dynamic impact loading by 50%. A similar effect of the addition of nitrogen was found for Ti–B–N coatings [41]. The positive influence of nitrogen can be explained by an increased
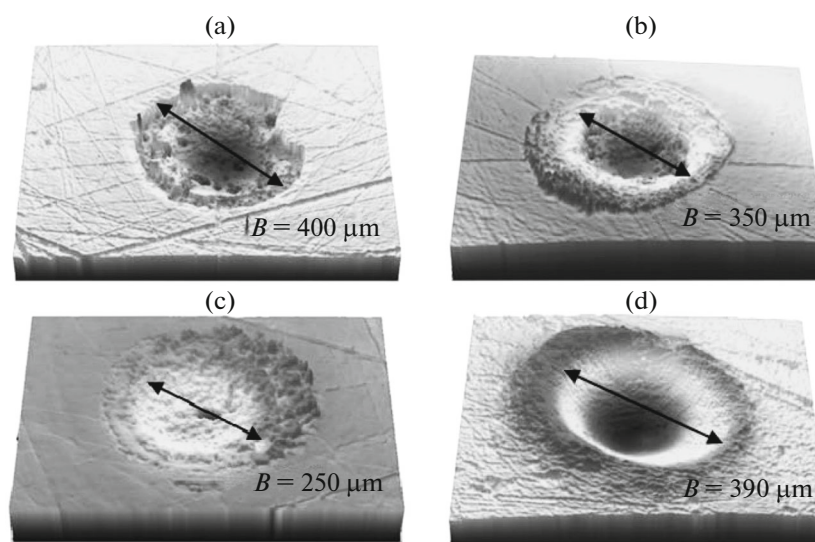

(a) $B = 400$ μm (b) $B = 350$ μm (c) $B = 250$ μm (d) $B = 390$ μm

Fig. 7. 3D profiles of craters for the coatings (a) *1*, (b) *2*, (c) *3*, and (d) for the substrate.

Table 3. Results obtained in the dynamic impact tests of coatings

Sample no.	Medium	D, μm	B, μm	$V \times 10^{-3}$, μm^3
1	Ar	2.63	400	54.1
2	Ar + 15% N$_2$	2.50	350	49.0
3	N$_2$	1.85	250	26.9

cracking resistance and viscosity of the films [42]. Note that the volume of the crater in the substrate ($V = 141.7 \times 10^3$ μm^3) is 2.6, 2.9, and 5.3 times larger than the values found for the coatings of *1*, *2*, and *3*, respectively.

CONCLUSIONS

Coatings of the Zr−B−N system obtained by HIPIMS technology had a dense structure without prominent columnar elements. The addition of nitrogen led to a decrease in the grain size of *h*-ZrB$_2$ and to the amorphization of the coatings.

Raman and infrared spectroscopic methods revealed that the BN phase appears upon depositions in the nitrogen-containing medium, which somewhat affects the mechanical characteristics, but has a positive influence on the tribological and optical properties of the coatings. For the nonreactive coatings, the hardness of 19 GPa and elastic modulus of 221 GPa were measured; these values are 47 and 37% lower, respectively, upon the addition of nitrogen.

Increasing nitrogen content resulted in the growth of the optical transmittance up to 97% in the wavelength range of 350−950 nm.

When the coatings are deposited in the atmosphere of N$_2$, the initial sliding coefficient decreased by ~60% with the counterobject made from SUS316 steel. Dynamic impact load tests showed the increase in the wear resistance by 50% when nitrogen was introduced into the coatings. The coatings obtained by the HIPIMS method possessed better adhesion strength when compared to the samples deposited by DCMS.

ACKNOWLEDGMENTS

FUNDING

REFERENCES

1. Rau, J.V., Ferro, D., Falcone, M.B., Generosi, A., Rossi Albertini, V., Latini, A., Teghil, R., and Barinov, S.M., Hardness of zirconium diboride films deposited on titanium substrates, *Mater. Chem. Phys.,* 2008, vol. 112, pp. 504−509.

2. Magnuson, M., Tengdelius, L., Greczynski, G., Hultman, L., and Högberg, H., Chemical bonding in epitaxial ZrB$_2$ studied by X-ray spectroscopy, *Thin Solid Films,* 2018, vol. 649, pp. 89−96.

3. Reich, S., Suhr, H., Hankó, K., and Szepes, L., Deposition of thin films of zirconium and Hafnium Boride by plasma enhanced chemical vapor deposition, *Adv. Mater.,* 1992, vol. 4, pp. 650−653.

4. Zhang, M., Ma, X., Yin, J., Zhang, Y., Zhang, L., Zhou, Y., Feng, X., Li, W., Wang, X., Chen, H., Zhang, L., Yin, L., and Deng, L., Experimental and theoretical modeling study on the infrared properties of ZrB$_2$ thin film, *Thin Solid Films,* 2020, vol. 709, article no. 138140.

5. Kiryukhantsev-Korneev, Ph.V., Lemesheva, M.V., Shvyndina, N.V., Levashov, E.A., and Potanin, A.Yu., Structure, mechanical properties, and oxidation resistance of ZrB$_2$, ZrSiB, and ZrSiB/SiBC coatings, *Prot. Met. Phys. Chem. Surf.,* 2018, vol. 54, no. 6, pp. 1147−1156.

6. Tengdelius, L., Broitman, E., Lu, J., Eriksson, F., Birch, J., Nyberg, T., Hultman, L., and Högberg, H., Hard and elastic epitaxial ZrB$_2$ thin films on Al$_2$O$_3$ (0001) substrates deposited by magnetron sputtering from a ZrB$_2$ compound target, *Acta Mater.,* 2016, vol. 111, pp. 166−172.

7. Gao, X.-H., Qiu, X.-L., Li, X.-T., Theiss, W., Chen, B.-H., Guo, H.-X., Zhou, T.-H., and Liu, G., Structure, thermal stability and optical simulation of ZrB$_2$ based spectrally selective solar absorber coatings, *Sol. Energy Mater. Sol. Cells,* 2019, vol. 193, pp. 178−183.

8. Sun, Y., Xiao, X., Chai, G., Xu, G., Xiong, B., and Zhang, S., Microstructure, optical properties and thermal stability of ZrB$_2$ and Zr−B−N thin films as high-temperature solar selective absorbers, *Mater. Express,* 2014, vol. 4, no. 3, pp. 205−212.

9. Qiu, X.-L., Gao, X.-H., He, C.-Y., and Liu, G., Optical design, thermal shock resistance and failure mechanism of a novel multilayer spectrally selective absorber coating based on HfB$_2$ and ZrB$_2$, *Sol. Energy Mater. Sol. Cells,* 2020, vol. 211, article no. 110533.

10. Dong, Y., Wang, T.-G., Yan, B., Qi, H.-J., Guo, Y.-Y., and Xu, S.-S., Study on the microstructure and mechanical properties of Zr−B−(N) tool coatings prepared by hybrid coating system, *Procedia Manuf.,* 2018, vol. 26, pp. 806−817.

11. Ramana, J.V., Kumar, S., David, C., Ray, A.K., and Raju, V.S., Characterization of zirconium nitride coatings prepared by DC magnetron sputtering, *Mater. Lett.,* 2000, vol. 43, pp. 73−76.

12. Kiryukhantsev-Korneev, Ph. and Levashov, E., Transparency effect in Zr−B−N coatings obtained by magnetron sputtering of ZrB$_2$ target, *Tech. Phys. Lett.,* 2020, vol. 46, pp. 179−181.

13. Übleis, A., Mitterer, C., and Ebner, R., Optical properties and corrosion behaviour of sputtered Zr−B and Zr−B−N coatings, *Surf. Coat. Technol.,* 1993, vol. 60, pp. 571−576.

14. Meng, Y., Song, Z.X., Li, Y.H., Qian, D., Hu, W., and Xu, K.W., Thermal stability of ultra thin Zr−B−N films as diffusion barrier between Cu and Si, *Appl. Surf. Sci.,* 2020, vol. 527, article no. 146810.

15. Holzschuh, H., Deposition of Ti-B-N (single and multilayer) and Zr−B−N coatings by chemical vapor deposition techniques on cutting tools, *Thin Solid Films,* 2004, vols. 469−470, pp. 92−98.

16. Dong, Y., Wang, T., Guo, Y., Li, J., and Wan, W., Effect of N$_2$-flow rate and annealing temperature on properties Zr−B−N nano-composite coatings, *J. Vac. Sci. Technol.,* 2018, vol. 38, no. 3, pp. 214−220.

17. Deng, Y., Chen, W., Li, B., Wang, C., Kuang, T., and Li, Y., Physical vapor deposition technology for coated cutting tools: A review, *Ceram. Int.,* 2020, vol. 46, pp. 18373−18390.

18. Kim, H.T., Jung, S.K., and Lee, S.-Y., Properties of ITO films deposited on paper sheets using a low-frequency (60 Hz) DC-pulsed magnetron sputtering method, *Vacuum,* 2021, vol. 187, article no. 110056.

19. Chung, C.K., Chen, T.S., Chang, N.W., Chang, S.C., and Liao, M.W., Oxidation resistance and mechanical property of cosputtered quasi-amorphous Ta−Si−N films under vacuum rapid thermal annealing, *Surf. Coat. Technol.,* 2020, vol. 205, pp. 1268−1272.

20. Sarakinos, K., Alami, J., and Konstantinidis, S., High power pulsed magnetron sputtering: A review on scientific and engineering state of the art, *Surf. Coat. Technol.,* 2010, vol. 204, pp. 1661−1684.

21. Kiryukhantsev-Korneev, Ph.V., Sheveyko, A.N., Vorotilo, S.A., and Levashov, E.A., Wear-resistant Ti−Al−Ni−C−N coatings produced by magnetron sputtering of SHS-targets in the DC and HIPIMS modes, *Ceram. Int.,* 2020, vol. 46, no. 2, pp. 1775−1783.

22. Ghailane, A., Makha, M., Larhlimi, H., and Alami, J., Design of hard coatings deposited by HIPIMS and DCMS, *Mater. Lett.,* 2020, vol. 280, article no. 128540.

23. Ghailane, A., Larhlimi, H., Tamraoui, Y., Makha, M., Busch, H., Fischer, C.B., and Alami, J., The effect of magnetic field configuration on structural and mechanical properties of TiN coatings deposited by HIPIMS and DCMS, *Surf. Coat. Technol.,* 2020, vol. 404, article no. 126572.

24. Mitterer, C., Uebleis, A., and Ebner, R., Sputter deposition of wear resistant coatings within the system Zr−B−N, *J. Mater. Sci. Eng.,* 1991, vol. 140, nos. 1−2, pp. 670−675.

25. Kiryukhantsev-Korneev, Ph.V. and Sytchenko, A.D., The influence of H, W, H/E, H^3/E^2, structure and chemical composition on the resistance of Ti−B−(N), Mo−B−(N), Cr−B−(N), and Zr−B−(N) coatings to cyclic impact loading, *Prot. Met. Phys. Chem. Surf.,* 2020, vol. 56, no. 6, pp. 1190−1200.

26. Urgen, M., Cakir, A.F., Eryilmaz, O.L., and Mitterer, C., Corrosion of zirconium boride and zirconium boron nitride coated steels, *Surf. Coat. Technol.,* 1995, vol. 71, no. 1, pp. 60−66.

27. Kuznetsova, T., Lapitskaya, V., Khabarava, A., Chizhik, S., Warcholinski, B., and Gilewicz, A., The influence of nitrogen on the morphology of ZrN coatings deposited by magnetron sputtering, *Appl. Surf. Sci.,* 2020, vol. 522, article no. 146508.

28. Liu, Z.-J., Xing, X.-J., Jiang, X.-Y., Wang, X., Zhang, L., Jian, X., Mu, C.-H., Han, T.-C., Lu, H.-P., Zhang, L.-B., Yin, L.-J., and Deng, L.-J., Structural self-deterioration mechanism for zirconium diboride in an inert environment, *Ceram. Int.,* 2021, vol. 47, pp. 18977−18983.

29. Mokgadi, T.F., Madito, M.J., Mlambo, M., Skuratov, V.A., Motloung, S.V., and Hlatshwayo, T.T., Slow and swift heavy ions irradiation of zirconium nitride (ZrN) and the migration behaviour of implanted Eu, *Nucl. Instrum. Methods Phys. Res., Sect. B,* 2019, vol. 461, pp. 63−69.

30. Ben el Mekki, M., Djouadi, M.A., Guiot, E., Mortet, V., Pascallon, J., Stambouli, V., Bouchier, D., Mestres, N., and Nouet, G., Structure investigation of BN films grown by ion-beam-assisted deposition by means of polarized IR and Raman spectroscopy, *Surf. Coat. Technol.,* 1999, vols. 116−119, pp. 93−99.

31. Zhong, B., Zhang, T., Huang, X.X., Wen, G.W., Chen, J.W., Wang, C.J., and Huang, Y.D., Fabrication and Raman scattering behavior of novel turbostratic BN thin films, *Mater. Lett.,* 2015, vol. 151, pp. 130−133.

32. Pokropivny, V., Kovrygin, S., Gubanov, V., Lohmus, R., Lohmus, A., and Vesi, U., *Ab-initio calculation of Raman spectra of single-walled BN nanotubes, Phys. E (Amsterdam, Neth.),* 2008, vol. 40, pp. 2339−2342.

33. Kiryukhantsev-Korneev, Ph.V., Pierson, J.F., Bychkova, M.Ya., Manakova, O.S., Levashov, E.A., and Shtansky, D.V., Comparative study of sliding, scratching, and impact-loading behavior of hard CrB$_2$ and Cr−B−N films, *Tribol. Lett.,* 2016, vol. 63, article no. 44.

34. Yamauchi, S. and Do, S., Raman spectroscopic study on the behavior of boric acid in wood, *J. Wood Sci.,* 2003, vol. 49, pp. 227−234.

35. Zhao, S., Zhao, Y., Ran, Y., Lu, H., Guo, Q., Gao, C., Zhao, Y., Yan, W., Jiang, Z., Wu, H., Zhang, D., and Wang, Z., Surface enhanced Raman scattering on ion-beam-deposited TiN$_x$/Si substrates, *Nucl. Instrum. Methods Phys. Res., Sect. B,* 2020, vol. 472, pp. 24−31.

36. Li, H., Yang, B., Yu, B., Huang, N., Liu, L., Lu, J., and Jiang, X., Graphene-coated Si nanowires as substrates for surface-enhanced Raman scattering, *Appl. Surf. Sci.,* 2021, vol. 541, article no. 148486.

37. Wang, X., Ji, Y., Zhang, M., Zhao, Y., Chen, Y., Zhao, Z., Pan, S., and Wang, H., Damage effects in in 6H-SiC single crystals by Si&H dual ion irradiation: A combined Raman and XRD study, *Nucl. Instrum. Methods Phys. Res., Sect. B,* 2020, vol. 485, pp. 20−25.

38. Yu, L., Zhao, H., and Xu, J., Mechanical, tribological and corrosion performance of WBN composite films deposited by reactive magnetron sputtering, *Appl. Surf. Sci.,* 2014, vol. 315, pp. 380−386.

39. Pat, S., Şilik, E., Musaoğlu, C., Özen, S., Mohammad-igharehbagh, R., Hakan Yudar, H., and Korkmaz, Ş., Cubic BN thin film deposition by a RF magnetron sputtering, *Vacuum,* 2018, vol. 157, pp. 31−35.

40. Podgornik, B., Kafexhiu, F., Kosec, T., Jerina, J., and Kalin, M., Friction and anti-galling properties of hexagonal boron nitride (*h*-BN) in aluminium forming, *Wear,* 2017, vols. 388−389, pp. 2−8.

41. Rebholz, C., Ziegele, H., Leyland, A., and Matthews, A., Structure, mechanical and tribological properties of Ti−B−N and Ti−Al−B−N multiphase thin films produced by electron-beam evaporation, *J. Vac. Sci. Technol., A,* 1998, vol. 16, pp. 2851−2857.

42. Kiryukhantsev-Korneev, Ph.V., Pierson, J.F., Kuptsov, K.A., and Shtansky, D.V., Hard Cr−Al−Si−B−(N) coatings deposited by reactive and non-reactive magnetron sputtering of CrAlSiB target, *Appl. Surf. Sci.,* 2014, vol. 314, pp. 104−111.

Translated by S. Efimov